A NEW APPROACH TO DESIGN GEOGRID REINFORCEMENT

M. Ziegler, V. Timmers
Geotechnical Engineering, Aachen University of Technology, Germany

ABSTRACT: Construction of slopes and retaining walls as geogrid reinforced ground compounds is of increasing importance. The dimensioning of the required anchor length of the reinforcement layers is based on the results of pull-out tests. Previous calculation methods as in the EBGEO for example act on the assumption of a linear distribution of tensile forces over the anchor length. For the chosen combination of geogrid and filling soil, test results attained at RWTH Aachen University of Technology show that this approach is conservative. Also, these results will show that the actual reduction takes place by more expeditious means. To be presented is a calculation model, with which the observed effects can be mapped to serve an economical dimensioning of the anchor length.

1 INTRODUCTION

Slopes and bearing constructions made of geogrid reinforced ground compounds are characterized by their adaptability to complex terrain, their economic efficiency due to little material expense, their high tolerance towards sub soil settlements as well as their high rigidity against static loads. The advantages compared to conventional design have already lead to an increasing acceptance towards solutions involving geogrid reinforced constructions. In practice, even slopes up to fifteen meters high have stood the test of time [Floss, 1999].

Tests have shown that the actual safety factor of slope stability is far greater than the calculated value. This suggests a minor degree of utilization 1/f of the reinforced elements during usage. The high bearing capacity cannot merely be explained by the frictional behavior between the building materials used. Apparently, additional resistance forces are mobilised by the complex interaction of the chosen reinforcement and the filling soil. This effect is not taken into account in current methods of calculation, as described among others by Jewell [Jewell, 1996].

2 EXPERIMENTS

2.1 *Experiment set-up*

A 30 cm ≈ 40 cm modified shear box was used to conduct pull-out experiments on a geogrid of high tensile stiffness, made of polyester Secugrid 40/40 Q6 by Naue Fasertechnik GmbH and furthermore on welded steel grids manufactured with a similar geometry. Several samples with differing numbers of cross bars and cross bar clearance have been used. As filling soil, a very dense sand was used. Fig. 1 displays a sketch of the experiment set-up.

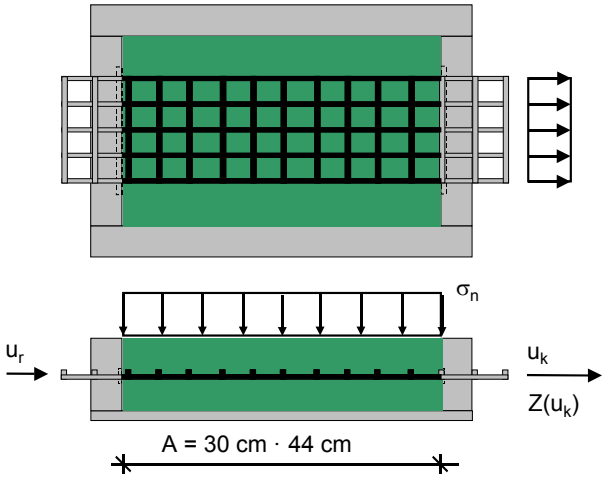

Figure 1 Experiment set-up

The pull-out-force Z, the pull-out-distance u_k at the clamp and at the rear end of the grid u_r were recorded with a fully electronized measuring data acquisition. All experiments were conducted several times, their results being averaged over.

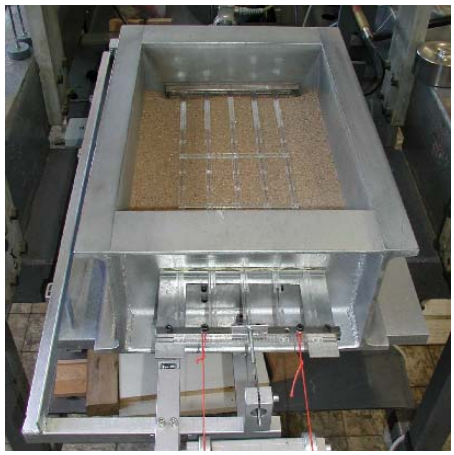

Figure 2 Pull-out box: rear side

2.2 *Characteristical test results*

Fig. 3 displays a characteristical test result for a grid without cross bars (S0- sample) and a grid with two cross bars (S2- samples) for pull-out distances u_k at the clamp up to 50 mm. With the S0- samples, the normal-stress dependant pull-out force maximum was reached after a few mm. Subsequently, a slight decrease in the afterwards constant pull-out-force occurred.

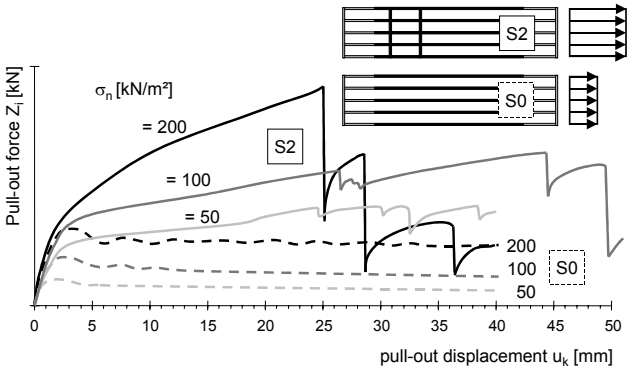

Figure 3 Typical test results

At first, the drag trajectories are equally steep with the S2- sample. However, no distinctive maxima could be identified in the following, the curves kept on ascending with a lower acclivity. The steady increase in force from that point onwards was only limited for greater pull-out-distances by exceeding the grid's tensile strength or the bearing capacity of the knods.

However, when conducting the pull-out, the force was increased due to the redistribution onto neighboring bars, suggesting a ductile behavior of the construct.

As seen in fig. 3, a few cross bars are sufficient to imply a significant boost in pull-out force. Apparently, this is due to the fact that the cross bars and the filling soil in front of it contribute to the load distribution. Permanent deformations on dismantled cross bars are a clear sign of considerable stress on these construction elements, affirming this assumption (fig. 4).

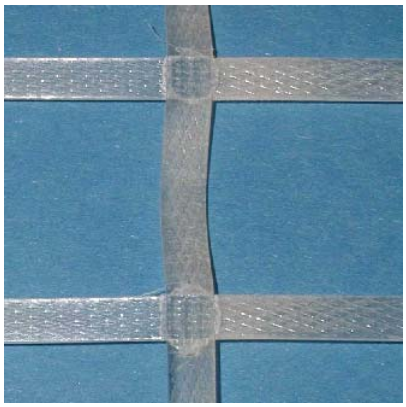

Figure 4 Permanent deformation of a geosynthetic grid

In order to visualize the importance of cross bar bearing effects, grids with a similar geometry have been made of steel. The permanent cross bar torsional deformations (fig. 5) are by far greater than those of geosynthetic bars, since there is no limiting factor in the rigidity of the welded steel knods.

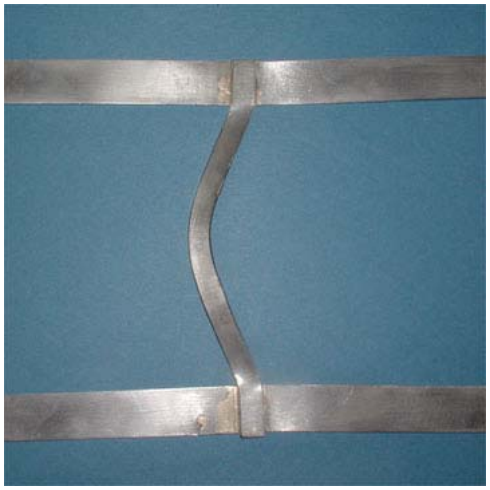

Figure 5 Permanent deformation of a welded steel specimen

3 CROSS BAR BEARING EFFECT QUANTIFICATION

To quantify the grid bar's bearing effect, systematic pull-out-experiments using 1,2 and 3 cross bars (S1, S2 and S3 configurations) were conducted. The measured drag forces on grids without cross bars served as a reference.

3.1 *S0- experiments*

During the S0- experiment analysis, the measured failure drag forces as well as the residual forces after 5 to 10 mm pull-out displacement were divided by the surface area of the grid bars' top- and bottom sides. The corresponding friction angles were φ_{S0f} = 23.3° (fig. 6) and φ_{S0r} = 20.1°, which is only 5 to 10% less than the results of direct shear tests using 6≈6 cm² filling soil samples. An adhesion could not be observed during the experiments.

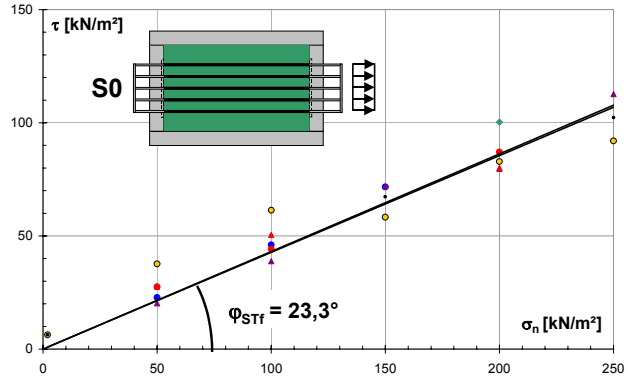

Figure 6 S0-experiments: shear stresses

3.2 *Plough factor*

Fig. 7 shows the displacement-dependant pull-out forces on S0-, S1 and S3- configurations, averaged over in several identical tests for different normal stresses. With regard to the relevant, small relative displacements between the reinforcement and the filling soil, the illustration was constricted to pull-out displacements of 12 mm from the clamp onwards.

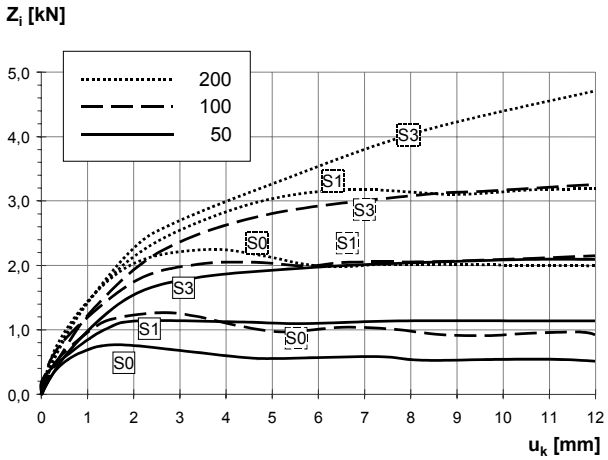

Figure 7 Pull-out forces vs. pull-out displacements of the clamp

After a movement of just a few millimetres, a single cross bar is sufficient to produce an increase in force ranging from 50% to 100% on S1- samples compared to S0- samples, even though the bar surface area has only increased by 7%. Thus, this enormous increase in force cannot be explained by surface friction between the grid bars and the filling soil alone.

A plough factor p_{Si} renders an illustration of the relative increase of the pull-out forces in dependence on the number of bars. p_{Si} is defined as pull-out force Z_{Si} on a grid configuration with i cross bars divided by the residual pull-out force Z_{S0r} on a S0- sample.

$$p_{Si}(\sigma_n) := \frac{Z_{Si}(u_k = 6\,\text{mm})}{Z_{S0r}} \qquad (1)$$

In each case, the drag forces are compared to one another after a clamp displacement u_k = 6 mm, the distance after which, for all the normal stresses tested, the S0-forces on the grids in question have already reached their residual value. Fig. 8 illustrates the plough factors for all tested grid geometries and normal stresses for a clamp displacement u_k = 6 mm.

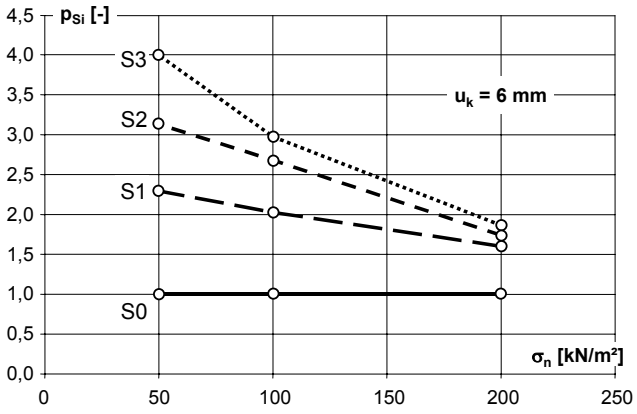

Figure 8 Plough factor vs. normal stresses

The plough factor increases with growing cross bar numbers. However, the force increase per cross bar decreases with growing numbers of cross bars in place. The more cross bars are in place, the smaller the growth due to an additional bar. The cross bar bearing effects are largest for minor normal stresses and decrease steadily with increasing normal stress.

4 CALCULATION MODEL

The drag force curve Z(x) in a certain reinforcement layer (fig. 9) is influenced by interface friction between the filling soil and the cross bars as well as by the drag force leaps ΔZ_i, which are inducted into the cross bars at the grid joints due to the absorbed soil resistance.

4.1 *Interface friction*

When pull-out strain is applied, the bond's roughness between the filling soil and the longitudinal bars result in the build up of shear stresses on the bars' surfaces. This causes a change in drag force in the longitudinal bar of the width b_{St}:

$$\frac{dZ(x)}{dx} = \tau_{St}(x) \cdot b_{St} \approx 2 \qquad (2)$$

The shear stress is dependant on the interface friction angle φ_{S0} between the geosynthetic and the soil (fig. 6) and is considered constant for a given normal stress over the bar length. Fig. 9 displays the resulting drag force curve which ascends steadily between the cross bars.

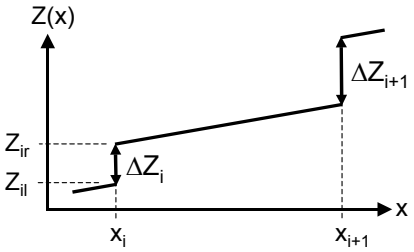

Figure 9 Leaps in drag force curve

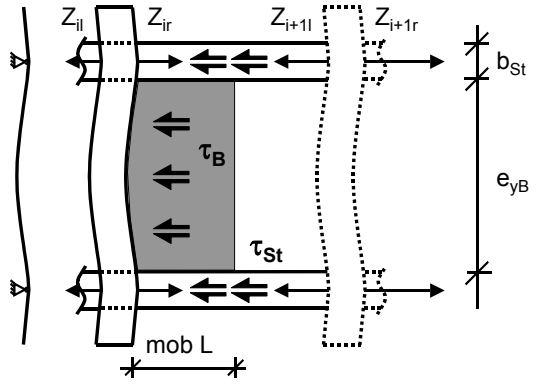

Figure 10 Interface shear, mobilised soil area

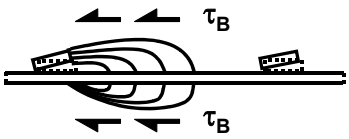

Figure 11 Mobilised soil area

4.2 *Soil resistance in front of the geogrid*

To explain the large cross bar bearing effects observed, a mechanical model was designed in which the cross

bar is being treated as a beam on two pillars (fig. 10). A slight cross-bar displacement u_{QSt} makes the filling soil rub against the top- and bottom side of the cross bar. Were the movement to be continued, the ground particles in front of the cross bar would wedge, being pushed ahead of the cross bar as by a plough.

Fig. 11 illustrates how the forces wedged into the granular structure by the cross bar are transferred to the surrounding soil via friction at the border areas of the restraint soil area. The soil resistance affecting the cross bar is the integral of the shear stress on the contribution area:

$$E_{pQ} = \int_A \tau_B dA \tag{3}$$

The shear stress τ_B is dependant on the soil's friction angle and the locally applicable normal stress:

$$\tau_B = \sigma_n \cdot \tan \varphi_B \tag{4}$$

Disregarding dilatancy effects, the normal stress is assumed to be equally dispersed over the bar surface and the filling soil in the grid spaces.

The soil resistance E_{pQ} in front of a cross bar i is inserted into the longitudinal bars in form of a drag force leap ΔZ_i at the grid joint

$$\Delta Z_i = E_{pQ} \tag{5}$$

which makes the drag force in the longitudinal bars leap from Z_{il} (left side of the grid joint) to Z_{ir} (right side).

4.3 *Mobilised soil area*

To grasp the soil resistance E_{pQ} in a calculative way, the soil area that is actually shifted after a given pull-out displacement u_{QSt} is simplified as a coextensive rectangle measuring mob A = e_{yB} ≈ mob L(u) (fig. 10), with e_{yB} being the width of the grid opening transverse the pull-out direction. As the normal stress applying to this area is constant, the shear stresses are also constant, rendering a description of the drag force leap possible:

$$\Delta Z_i = 2 \cdot \sigma_n \cdot \tan \varphi_B \cdot e_{yB} \cdot \text{mob L}(u) \tag{6}$$

The factor 2 represents the friction occuring on both the top and the bottom sides of the rectangle. As the pull-out displacement is growing, the only changing component in this equation is mob L. Therefore, the mobilised length mob L is a proportional scale for every cross bar's absorbed soil resistance and the drag force leap ΔZ_i.

Growing cross bar displacement results in growth of the contributing length mob L. However, this area can grow no more as soon as it touches the neighboring cross bar. Therefore, the bearing capacity of a single cross bar is limited by its distance to the adjacent bar. If pulled out further, the cross bars and the mobilised soil would slip through the surrounding filling soil.

Furthermore, the cross bar is subject to torsional deformations, increasing the shifted soil's thickness and raising the ploughing resistance.

The soil resistance resulting from the ploughing effect is considerable and is by far exceeding the interface friction between the grid and the filling soil.

4.4 *Mobilisation function*

The bearing capacity of single cross bars can be displayed by using the results of the pull out experiments on S1- and S0- samples (Fig. 7). Establishing the difference between the drag forces Z_1 and Z_0 as a function of pull-out displacement, the increase in pull-out force due to a single cross bar is

$$\Delta Z_1(u) = Z_1(u) - Z_0(u) \tag{7}$$

Using the proportional correlation between ΔZ_i and mob L according to (6), mob L can be determined from

$$\text{mob L}(u) = \frac{Z_1(u) - Z_0(u)}{2 \cdot \sigma_n \cdot \tan \varphi_B \cdot e_{yB}} \tag{8}$$

This way, a mobilisation function mob L(u) can be determined for every normal stress tested. The resulting graphs are displayed for clamp displacements up to u_k = 6 mm in fig. 12.

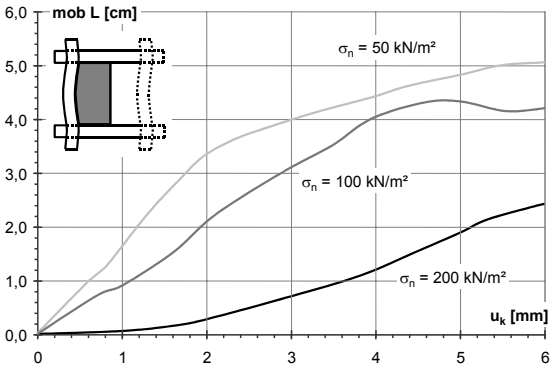

Figure 12 Mobilisation function vs. clamp displacement

If one compared the curves at the same clamp displacement, the mobilised areas decrease with increasing normal stress. Thus, the contribution to the overall pull-out resistance of the soil shifted ahead of every single cross bar decreases in this diagram. This observation corresponds to the plough factor displayed in fig. 8.

It is striking that, after just a few millimetres of clamp displacement, the mobilised area reaches the cross bar distance of 4 cm. If this was applied to a full grid (one with all cross bars in place) the full opening width of the first grid would contribute to the pull-out resistance after just a few mm of displacement.

4.5 *Longitudinal grid strain influence*

The reason for the granular structure's restraint is not actually the clamp displacement u_k, but the actual displacement u_{QSt} of the grid bar. The actual displacement u_{QSt} can be determined from the clamp displacement u_k and grid strain $\varepsilon_x(x)$, which can be taken from the characteristic stress-strain curve (fig. 13) if the tensile stress distribution $\sigma_x(x)$ is known.

Figure 13 Bilinear idealization of characteristic geogrid stress-strain curve

$$u_{QSt}(u_k) = u_K - \int_{x_{QSt}}^{x_K} \varepsilon_x(x)dx \qquad (9)$$

Fig. 14 displays the linear drag force distribution in S0-grids, assuming a constant shear stress insertion into the longitudinal bars.

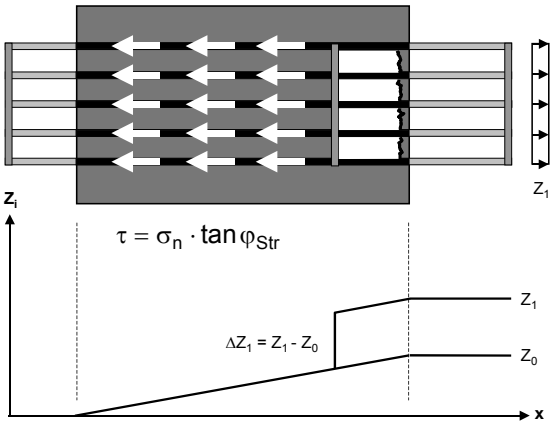

Figure 14 Drag force distribution of S0- / S1- specimen

At the rear end, the grids drag force equals zero. Thus, the drag force distribution can also be applied with the same gradient from the rear box slot upto the cross bar. The unknown drag force leap occuring at the cross bar ΔZ_i can be read off the graph as the difference between drag forces on the left and the right side of the cross bar. The resulting drag force distribution is displayed in fig. 14.

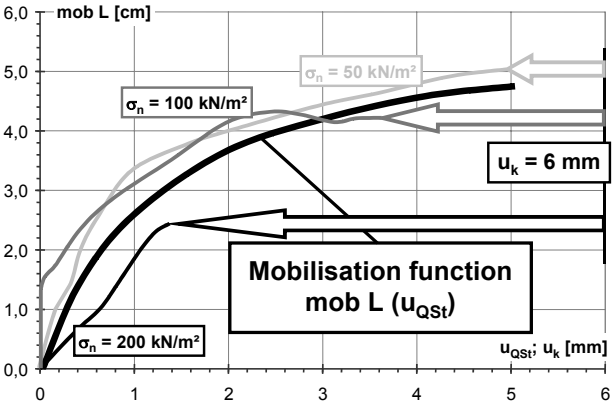

Figure 15 Mobilisation function vs. cross bar displacement

Fig. 15 displays the mobilisation function vs. the true cross-bar displacement. A clamp displacement of u_k = 6 mm causes clearly lower values of 5, 3.6 and 1.4 mm for the cross bar displacement, the lowest value being the result of the highest normal stress.

Transferring these corrections into the plough factor diagram (fig. 8) clarifies that the great plough factor decrease for high normal stress is predominantly caused by the fact that with a clamp displacement of u_k = 6 mm, the actual cross bar displacement is lower when major normal stress is applied than with a lower normal stress.

The graphs of the adjusted mobilisation functions virtually coincide for the minor normal stresses. Though lower values have resulted from applying σ_n = 200 kN/m², a normal-stress independant, mutual mobilisation function as an average of the three curves is assumed.

4.6 *Drag force curve in full grids*

In grids with more than one cross bar, the rear cross bars cause slighter drag force leaps than the ones in the front. Due to the strong drag forces occurring in that area, the grid's front is distended rather heavily. Therefore, the front bar is subject to a distinctly lesser displacement than the clamp. Moreover, the longitudinal grid strain between the first and the second cross bar results in the second bar being subjected to smaller displacements. The further behind the cross bars are, the lesser are their displacements and the smaller is the soil area mobilised. Thus, the cross bar's loads decrease continuously in the rear area.

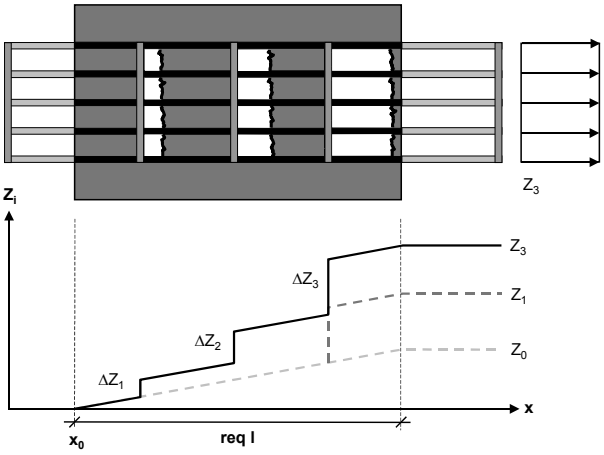

Figure 16 drag force curve on a full grid

This effect, which is not considered by EBGEO [DGGT, 1997], wears on up to the point x_o from which on the grid is no longer subject to significant displacement since no more loads are transferred by the cross bars. Not taking any safety factors into consideration, the distance from the place of pull-out force induction to the point x_o equals the required anchor length req l of the reinforcement in the rear soil area.

Starting the calculation of the unknown grid displacements u(x) and drag forces $Z_i(x)$ from the rear end x_o of the grid allows for a description of the possible pull-out force $Z_i(x)$ as a function of u(x) for every place x.

5 DIMENSIONING NOMOGRAM

The mechanical correlations between the variables Z(x), $\varepsilon_x(x)$ and u(x) explained above allow for a step by step determination of these values. The following dimensioning diagram (fig. 17) was developed on that purpose.

The nomogram's left part represents the grid's longitudinal axis. The undetermined displacement u(x) and the strain $\varepsilon_x(x)$ are displayed in the upper left, the grid drag force Z(x) in the lower left part.

$Z_i(x)$ starts at zero and its gradient between the cross bars is given by the known interface shear stress. Its distribution can thus be calculated and displayed up to the first cross bar (i=1). The according strains $\varepsilon_x(x)$ can be taken from the characteristic geogrid stress-strain curve and are displayed in the upper left part of the nomogram. They also start at zero on the rear end of the grid.

In order to determine the grid displacement distribution u(x), the strains have to be integrated with the grid front's displacement $u_0 = u(x=0)$ still being an undetermined boundary condition. If u_0 is set to 0, the grid is

subject to strain, but is not yet moved in the left end. Given any chosen u_0, the grid displacement u_1 of the first cross bar can be determined.

Applied in the right part of the nomogram are the soil mechanical correlations between the mobilised length mob L on the abscissa, the grid displacement u and the drag force leaps ΔZ. In the upper right part, the specific mobilisation function is applied over the actual cross bar displacement u_{QSt}, the axis being switched in comparison to fig. 15. In the lower right part, the transmission function graphs according to (6) are displayed, determining the drag force leap ΔZ corresponding to a given value mob L in dependance of the normal stress applied.

The displacement u_1 of the first cross bar serves as an entry value for the mobilisation function. Its abscissa shows the soil area shifted by the first cross bar.

Taking this mob L value, one goes down onto the graph of the transmission function corresponding to the actually occurring normal stress, reading off the respective drag force leap ΔZ_1 on the ordinate. This is attached to the drag force distribution below left. Having finished the first step of calculation, the three unknown values $\varepsilon_x(x)$, u(x) and Z(x) are now determined for the area between the grid front and the first cross bar.

During the second step of calculation, the drag force distribution is prolonged up to the second cross bar with the same gradient determined from the interface friction. As it is shown in the nomogram's upper left part, the strain and displacement curves can thus be applied up to the second cross bar, making the bar's displacement u_2 known. It is larger than u_1. Transferring this to the mobilisation function and the fitting transmission function determines the drag force leap ΔZ_2 at the second cross bar, which turns out to be larger than ΔZ_1 at the first one.

To verify the experiment results, this method of calculation is repeated for every cross bar in place, until the front end of the grid or the clamp respectively is reached. If the displacement at the open grid end is preselected for a given construction situation, one can determine either the grid length for a given force to be absorbed or determine the absorbable force for a given grid length.

6 SUMMARY AND FUTURE PROSPECTS

With the calculation model presented here, it is rendered possible to use the available knowledge on the complex interaction between the reinforcement and the filling soil in a quantitative way in order to determine the necessary dimensions of the geogrid anchor length.

The model seems to apply to all types of grid and soil. To prove this and to significantly broaden the available database, further experiments are needed. Pull-out tests on steel grids in sand and in gravel are currently being conducted to trace the cross bar's bearing effects.

The course of calculation described, in which similar calculations are repeated in great numbers, is basically suited for computer automatization. Using these results, the enhancement of existing reinforcement products could be optimised in order to obtain a more cost-effective dimensioning and construction of geogrid reinforced ground compounds.

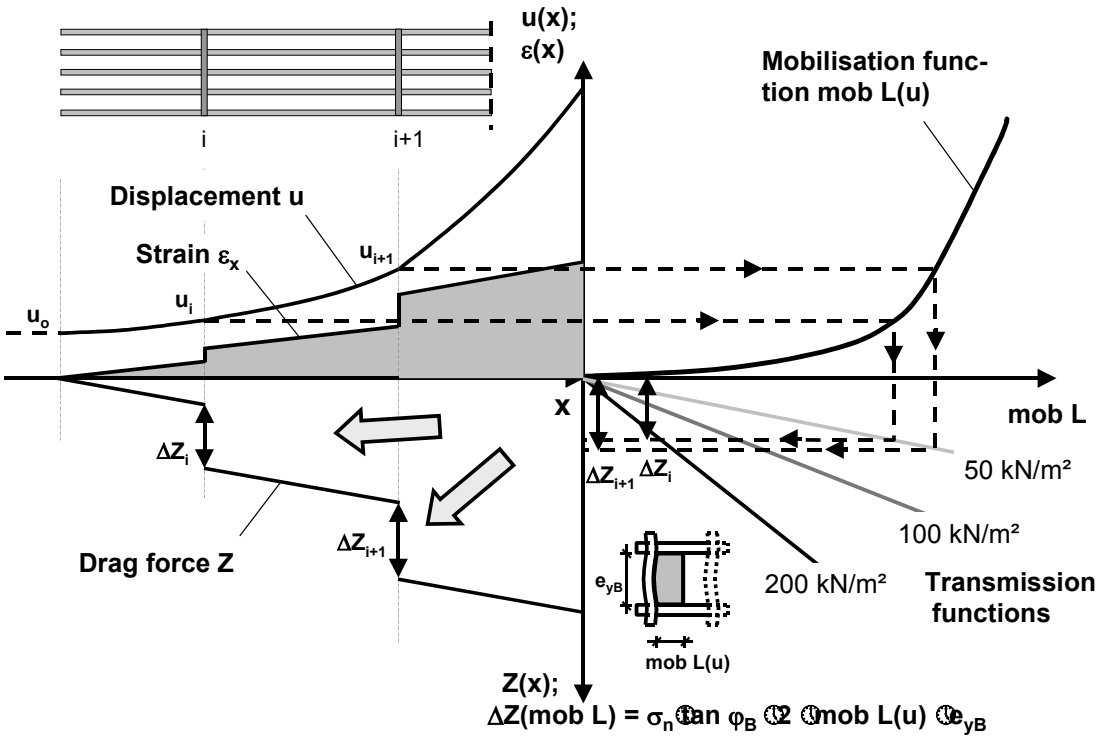

Figure 17 Dimensioning nomogram

7 REFERENCES

DGGT: Empfehlungen für Bewehrungen aus Geokunststoffen - EBGEO, Ernst & Sohn 1997

Floss, R.: Geogitterbewehrte Steilböschung am Hienberg (BAB A9 Nürnberg-Berlin). 6. Informations- und Vortragstagung über "Kunststoffe in der Geotechnik", 1999

Jewell, R.A.: Soil reinforcement with geotextiles. London, 1996